Rheologica Acta (2022) 61:415–425
https://doi.org/10.1007/s00397-022-01334-3

ORIGINAL CONTRIBUTION

Analysis of elongational flow of star polymers

Manfred H. Wagner[1] · **Esmaeil Narimissa**[2,3] · **Qian Huang**[4]

Received: 5 February 2022 / Revised: 7 March 2022 / Accepted: 7 March 2022 / Published online: 30 April 2022

Abstract
Star polymers with three arms are the simplest example of branched polymers. Elongational rheology data of three well-characterized monodisperse polystyrene melts, a symmetric star, an asymmetric star, and a linear polymer with the same span molecular weight of 180 kg/mol reported by Huang et al. (Macromolecules 49:6694−6699, 2016) are analyzed by the enhanced relaxation of stretch (ERS) model (Wagner and Narimissa, J Rheol 65:1413–1421, 2021). All three melts show the same elongational stress growth coefficient and the same steady-state elongational viscosity in fast extensional flows when the stretch-related Weissenberg number $Wi_R = \dot{\varepsilon}\tau_R > 1$. Excellent agreement between experimental data of elongational stress growth coefficient and model predictions is obtained, based exclusively on the linear-viscoelastic characterization of the polymer systems. Stress relaxation following steady elongational flow depends on the presence of the branch point and the length of the arm, and a new process regarding relaxation of the orientation of the stars is identified.

Keywords Polymer melt · Polystyrene · Star polymers · Elongation · Tube model · ERS model · Stretch relaxation · Relaxation of orientation

Introduction

Elongational viscosity measurements by use of filament stretching rheometers with locally-controlled deformation and deformation rate as developed by Hassager and coworkers (Bach al. 2003) have revealed surprising differences between the elongational rheology of linear polymer melts and their solutions (Huang et al. 2013, 2013). These differences were not foreseen by the original tube model of Doi and Edwards (1978, 1979), which is based on the assumption of a constant tube diameter a_0, and this has to lead to substantial modifications of the tube model as, e.g., discussed by Narimissa and coworkers (2019, 2020a,b, 2021) and Ianniruberto et al. (2020). According to Doi and Edwards (see Eq. A9 in Doi and Edwards 1978), the line density of monomer units that are found per length of the tube is a well-defined thermodynamic quantity defining the tube diameter. As a stretch of the test chain reduces the line density of monomers, this affects the value of the local tube diameter. Therefore, chain stretch at the mesoscopic level of the tube model is related to a strain-dependent tube diameter $a \leq a_0$, as first suggested by Marrucci and de Cindio (1980). Relaxing the assumption of constant tube diameter a_0 in nonlinear viscoelastic flow allowed for modelling of the elongational viscosity of monodisperse entangled linear polymer systems based exclusively on their linear-viscoelastic characterization and the Rouse stretch relaxation time of the chain (Wagner et al. 2005, 2021a,b; Narimissa et al. 2020a, 2021).

However, for other than linear polymers such as long-chain branched (LCB) polymer systems, progress in understanding the relation of molecular characteristics and nonlinear viscoelastic rheology has been rather limited, not least because of the scarcity of reliable rheological data for well-defined polymer systems. Nielsen et al. (2006) investigated

✉ Manfred H. Wagner
manfred.wagner@tu-berlin.de

✉ Esmaeil Narimissa
esmaeiln@technion.ac.il

[1] Polymer Engineering/Polymer Physics, Berlin Institute of Technology (TU Berlin), Ernst-Reuter-Platz 1, 10587 Berlin, Germany

[2] Department of Chemical Engineering, Technion–Israel Institute of Technology (IIT), Technion City, 32 000 Haifa, Israel

[3] Department of Chemical Engineering, Guangdong Technion–Israel Institute of Technology (GTIIT), Shantou 515063, China

[4] State Key Laboratory of Polymer Materials Engineering, Polymer Research Institute, Sichuan University, Chengdu 610065, China

the elongational viscosity of nearly monodisperse polystyrene (PS) pom-pom melt with two branch points and 2 to 3 arms per branch point, and they found elongational viscosity overshoot at the highest elongation rate. Wagner and Rolón-Garrído (2008) modified the molecular stress function (MSF) model by considering branch point withdrawal and obtained an agreement with the pom-pom polystyrene data of Nielsen et al. (2006). Huang et al. (2016) explored systematically the nonlinear dynamics of model branched polymers starting from the simplest structures, which are star polymers with three arms. They investigated three polystyrene melts, a symmetric star, an asymmetric star, and a linear polystyrene in nonlinear elongational flow. All three samples have the same span molecular weight of nominally 180 kg/mol and reach the same elongational steady-state viscosity in fast flows (faster than the inverse Rouse time), confirming the expectation of Ianniruberto and Marrucci (2013) that entangled melts of LCB macromolecules become quasilinear by aligning the arms in strong extensional flows. Indeed, Mortensen et al. (2018, 2021) could demonstrate by small-angle neutron scattering (SANS) studies of a three-armed polystyrene star polymer that upon exposure to large elongational flow, the star polymer indeed changes its conformation: all three arms are oriented parallel to the flow, one arm being either in positive or negative stretching direction, while the two other arms are oriented parallel, right next to each other in the direction opposite to the first arm. Huang et al. (2016) also measured stress relaxation following the steady elongational flow and found that the relaxation of the different samples depends on the presence of the branch point and the length of the arm.

In the present paper, we analyze the elongational viscosity data of Huang et al. (2016) by use of the ERS model, which has been recently developed in the context of tube models with varying tube diameters (Wagner and Narimissa 2021). The ERS model starts from the definition of the Rouse time being proportional to the square of the number of monomers in the chain. With increasing stretch and decreasing tube diameter a, the number of monomers in a control volume of length and diameter a will decrease with the consequence of enhanced relaxation of stretch in this control volume. The incremental increase of the relaxation rate with stretch is proportional to the 4th power of the stretch, and the evolution equation of the stretch is obtained as a balance of extension rate versus stretch relaxation rate. The ERS model leads to predictions of the elongational viscosity of linear polystyrene melts and solutions, which are in quantitative agreement with experimental evidence, based exclusively on the LVE characterization of the polymer systems and the Rouse time. It is of interest to see whether this model is also able to capture the dynamics of the simplest branched structures, i.e., star polymers.

The paper is organized as follows: we first give a short report of the experimental data and the linear-viscoelastic characterization of the polymer systems considered in the "Experimental data and linear-viscoelastic characterization" section, followed by a summary of the ERS model in the "Enhanced relaxation of stretch (ERS) model" section. The main focus of the paper is on the comparison of experimental data and model predictions for the start-up of elongational flow and for stress relaxation after the steady elongational flow. Conclusions are summarized in the last section.

Experimental data and linear-viscoelastic characterization

The three polystyrene melts with different molecular structures, a linear (Lin180), an asymmetric star (Star20), and a symmetric star (Star90), were synthesized via anionic polymerization. Lin180 has a molecular weight of 187 kg/mol, and the stars have a backbone of molecular weight of 185 kg/mol and an arm located at the centre of the backbone of molecular weight 20.5 kg/mol (Star20), and 92.4 kg/mol (Star90) (Huang et al. 2016), respectively. The molecular structures are illustrated in Figure 1, and the molecular characteristics are summarized in Table 1.

Details of small amplitude oscillatory spectroscopy (SAOS) and elongational viscosity measurements are presented in Huang et al. (2016). Elongational measurements using a filament stretching rheometer were performed at $T =$ 130°C. Storage (G') and loss modulus (G'') were measured at temperatures between 130 and 160 °C and shifted to $T_0 =$ 130 °C by time-temperature shifting (TTS) according to the WLF equation with shift factor a_{Tg},

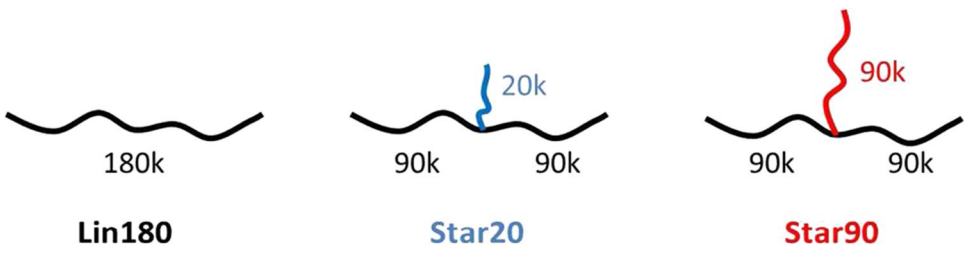

Fig. 1 Illustration of molecular structures for Lin180, Star20, and Star90. Reprinted with permission from Huang et al. (2016). Copyright [2016], American Chemical Society

Table 1 Sample characterization at $T = 130$ °C

Characteristics	Lin180	Star20	Star90
M_w [kg/mol]	187.0	208.3	289.1
M_w/M_n	1.02	1.03	1.03
Number of long arms	-	2	3
M_w [kg/mol] of long arm	-	92.4	92.4
M_w [kg/mol] of short arm	-	20.5	-
η_0 [Pa.s]	6.81e + 7	7.83e + 7	1.73e + 8
ϕ [-]	1	0.89	1
τ_d [s]	752	1563	3504
τ_R [s]	132	132	132
τ_d/τ_R	6	12	27

Table 2 Relaxation spectra at $T = 130$ °C by IRIS (Winter and Mours 2006)

Lin180		Star20		Star90	
g_i [Pa]	τ_i [s]	g_i [Pa]	τ_i [s]	g_i [Pa]	τ_i [s]
3.47e + 7	6.89e − 4	3.63e + 8	5.50e − 5	9.56e + 7	1.94e − 4
8.28e + 5	1.70e − 2	1.31e + 6	7.75e − 3	2.50e + 6	5.14e − 2
3.07e + 5	1.04e − 0	4.10e + 5	4.44e − 2	6.33e + 4	1.69e + 2
1.17e + 5	6.34e − 1	1.65e + 5	2.25e − 1	6.64e + 4	5.21e + 0
5.71e + 4	3.97e + 0	7.60 + 4	1.10e + 0	4.95e + 4	3.40e + 1
5.30e + 4	2.17e + 1	4.97e + 4	5.10e + 0	4.98e + 4	7.28e + 2
6.25e + 4	1.12e + 2	4.35e + 4	2.14e + 1	3.24e + 4	3.08e + 3
7.99e + 4	5.88e + 2	4.28e + 4	1.02e + 2	2.05e + 3	1.14e + 4
6.98e + 3	1.81e + 3	3.97e + 4	3.96e + 2		
		3.30e + 4	1.58e + 3		
		6.70e + 2	7.05e + 3		

$$\log_{10} a_{Tg} = \frac{-c_1^0 (T - T_0)}{c_2^0 + (T - T_0)} \tag{1}$$

and coefficients $c_1^0 = 8.99$ and $c_2^0 = 81.53$ K. From the mastercurves of G' and G', parsimonious relaxation spectra were obtained,

$$G(t) = \sum_{i=1} g_i \exp\left(-t/\tau_i\right) \tag{2}$$

for characterization of the linear-viscoelastic relaxation modulus $G(t)$. The partial moduli g_i and relaxation times τ_i (Table 2) as determined by the IRIS software (Winter and Mours 2006) result in excellent agreement with the linear-viscoelastic data of G' and G'', see Fig. 2.

From Figure 2a, it can be seen that the G' and G'' curves of Lin180 and Star90 overlap each other for frequencies $\omega > 0.1$ rad/s. This is essentially in accordance with the fact that a symmetric star polymer with arm mass M_a and a linear chain of mass $2M_a$ have the same Rouse time (Ianniruberto and Marrucci 2013). However, the G' and G'' curves of Lin180 and Star90 differ in the flow regime due to the branch point. Reptation is impossible for symmetric stars because the arms have no single tube down which to slide. As explained by Milner and McLeish (1997), stress relaxes in star melts by arm retraction combined with dynamic dilution. In the case of the asymmetric star, the short arm of Star20 is not well entangled (about one entanglement when taking the entanglement molar mass of PS as $M_{em} = 13.3$ kg/mol in the melt state) and thus relaxes much faster than the backbone. The asymmetric stars then looks like a linear chain composed of the two long arms, and the star can thus reptate (Frischknecht et al. 2002). In the viscoelastic regime, Star20 shows lower G' and G'' values than Star90 and Lin180, indicating that on the time scale of the backbone, the relaxed arm indeed behaves like a solvent that dilutes the backbone consisting of the two long arms with 92.4 kg/mol each. The volume fraction of the backbone of Star20 is given by (Table 1)

$$\phi = \frac{2 \cdot 92.4 \text{ kg/mol}}{M_w} = \frac{184.8}{208.3} = 0.89 \tag{3}$$

The dilution effect is also seen in the loss tangent $\tan\delta = G''/G'$ when plotted as a function of the absolute value of the complex modulus $G^* = \sqrt{G'^2 + G''^2}$ (Fig. 2b). Due to dilution, the minimum of $\tan\delta$ indicating the plateau modulus G_N of the polymer system is shifted to the left relative to the minima of Lin180 and Star90, showing a reduction of the plateau modulus. However, in the flow regime, Star20 shows higher G' and G'' values than Lin180 because the short arm increases the drag on the remaining two arms as they reptate.

According to the Doi–Edwards model, the Rouse time τ_R, the disengagement (or reptation) time τ_d and the zero-shear viscosity η_0 of linear chains with Z entanglements are given by (Dealy et al. 2018),

$$\tau_R = Z^2 \tau_e \tag{4}$$

$$\tau_d = 3Z\tau_R \tag{5}$$

$$\eta_0 = \frac{\pi^2}{12} G_N \tau_d \tag{6}$$

τ_e is the entanglement segment equilibration time. We identify here τ_d with the mean quadratic average of the relaxation times of the discrete relaxation spectrum and calculate η_0 from the discrete relaxation spectrum,

$$\tau_d = \frac{\sum_i g_i \tau_i^2}{\sum_i g_i \tau_i} \tag{7}$$

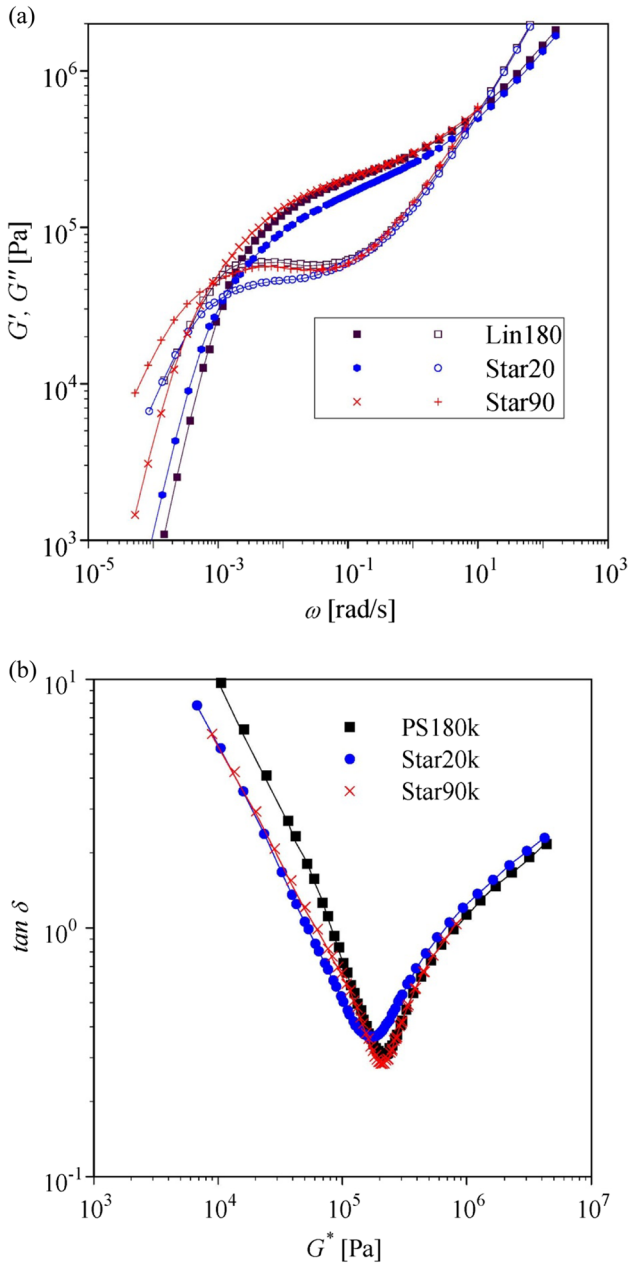

Fig. 2 **a** Storage (G') and loss modulus (G'') of Lin180, Star20, and Star90. Reprinted (adapted) with permission from Huang et al. (2016). Copyright [2016], American Chemical Society. **b** Loss tangent $\tan\delta = G''/G'$ as a function of the complex modulus G^*. Lines in (a) and (b) are fit by parsimonious spectra (Table 2)

$$\eta_0 = \sum_i g_i \tau_i \tag{8}$$

For quantification of the Rouse time τ_R, Osaki's approach (Osaki et al. 1982; Takahashi et al. 1993; Isaki et al. 2003; Menezes and Graessley 1982) is used, which extrapolates the Rouse time of unentangled polymer systems to the Rouse time of entangled polymer melts and solutions, and takes into account the power of 3.4 scaling of the zero-shear viscosity with molar mass M and polymer fraction ϕ. This leads to the relation (Wagner 2014).

$$\tau_R = \frac{12\, M\eta_0}{\pi^2 \rho\ \ RT\phi}\left(\frac{M_{\mathrm{cm}}}{M\phi}\right)^{2.4} \tag{9}$$

for the Rouse stretch relaxation time. M_{cm} denotes the critical molar mass in the melt state, when the entanglement effect becomes apparent by a change of the power of 1 to the power of 3.4 scaling of the zero-shear viscosity as a function of molar mass. For monodisperse polystyrene a value of $M_{\mathrm{cm}} = 35$ kg/mol has previously been used successfully for modeling the transient and steady-state elongational and shear viscosities of well-entangled linear PS melts and solutions of linear PS (Wagner 2014; Narimissa et al. 2020a, b, 2021; Wagner et al. 2021a, b). For Lin180, it is necessary to use a value of $M_{\mathrm{cm}} = 42.5$ kg/mol in Eq. (9) resulting in $\tau_R = 132s$ in order to obtain good agreement with the experimental elongational viscosity data. This may be due to the relatively low molecular weight of Lin180 and is still within the accepted range of $M_{\mathrm{cm}} \cong 2$ to $3M_{\mathrm{em}}$. Following Ianniruberto and Marrucci (2013), we assume that the stretch relaxation times of Star 20 and Star90 are identical to the Rouse stretch relaxation time of Lin180, i.e., $\tau_R = 132s$. The values of disengagement time, stretch relaxation time, and zero-shear viscosity as calculated from Eqs. (7–9) are summarized in Table 1. We note for later use that the ratio of disengagement time to Rouse or stretch relaxation time, τ_d/τ_R, increases from 6 (Lin180) to 12 (Star20) and 27 (Star90) due to the presence of the branch point, which suppresses reptation and restricts tube renewal to arm retraction by fluctuations, the more so, the longer the arm.

The enhanced relaxation of stretch (ERS) model

The MSF model is a generalized tube segment model with strain-dependent tube diameter (Wagner 1990; Wagner and Schaeffer 1992; Wagner et al. 2001, 2003, 2005; Narimissa and Wagner 2019). The extra stress tensor $\sigma(t)$ of the MSF model is given by a history integral of the form

$$\sigma(t) = \int_{-\infty}^{t} \frac{\partial G(t-t')}{\partial t'} f^2(t,t')\ \mathbf{S}_{\mathrm{DE}}^{\mathrm{IA}}(t,t')dt' \tag{10}$$

t is the time of observation when the stress is measured, and t' indicates the time when a tube segment was created by reptation. The strain measure $\mathbf{S}_{DE}^{IA}$ represents the contribution to the extra stress tensor originating from the affine rotation of the tube segments according to the

"independent alignment (IA)" assumption of Doi and Edwards (1978, 1979), and is given by

$$\mathbf{S}_{\mathrm{DE}}^{\mathrm{IA}}(t,t') \equiv 5\left\langle \frac{\mathbf{u}'\mathbf{u}'}{u'^2} \right\rangle_{\mathrm{o}} = 5\mathbf{S}(t,t') \tag{11}$$

with $\mathbf{S}(t,t')$ being the relative second order orientation tensor. $\mathbf{u}'\mathbf{u}'$ is the dyad of a deformed unit vector $\mathbf{u}' = \mathbf{u}'(t,t')$,

$$\mathbf{u}' = \mathbf{F}_t^{-1}\mathbf{u} \tag{12}$$

$\mathbf{F}_t^{-1} = \mathbf{F}_t^{-1}(t,t')$ is the relative deformation gradient tensor and u' is the length of $\mathbf{u}'$. The orientation average is indicated by $<\ldots>_0$,

$$\langle \ldots \rangle_{\mathrm{o}} \equiv \frac{1}{4\pi} \oint\!\!\oint [\ldots] \sin\theta_o d\theta_o d\phi_o \tag{13}$$

i.e., an average over an isotropic distribution of unit vectors $\mathbf{u}$.

$f = f(t,t')$ represents the inverse of the relative tube diameter a/a_0, and at the same time the relative length of a deformed tube segment,

$$f(t,t') = \frac{a_0}{a(t,t')} = \frac{l(t,t')}{l_0} \tag{14}$$

At time $t=t'$ the tube segment was created with equilibrium tube diameter a_0 and equilibrium length l_0. For $f \equiv 1$, Eq. (10) reduces to the original Doi–Edwards IA (DE IA) model.

While $\mathbf{S}_{\mathrm{DE}}^{\mathrm{IA}}$ is determined directly by the deformation history according to Eq. (11), f is found as a solution of an evolution equation considering affine tube segment deformation balanced by enhanced Rouse relaxation (Wagner and Narimissa 2021). With increasing stretch and decreasing tube diameter a, the number of monomers in a control volume of length and diameter a will decrease with the consequence of enhanced relaxation of stretch in this control volume. The incremental increase of the relaxation rate with stretch is proportional to the 4th power of the stretch, and the evolution equation of the ERS model is obtained as a balance of extension rate versus relaxation rate,

$$\frac{\partial f}{\partial t} = f(\mathbf{K} : \mathbf{S}) - \frac{f-1}{\tau_R}\left(1-\phi^4\right) - \frac{\phi^4\left(f^5-1\right)}{5\tau_R} \tag{15}$$

with initial condition $f(t,t'=0)=1$. In the limit of vanishing chain stretch, Eq. (15) degenerates naturally into the classical evolution equation,

$$\frac{\partial f}{\partial t} = f(\mathbf{K} : \mathbf{S}) - \frac{1}{\tau_R}(f-1) \tag{16}$$

Equations (10) and (15) represent the ERS model and are solved numerically. As shown by Wagner and Narimissa (2021), the ERS model and the extended interchain pressure (EIP) model (Wagner and Rolon-Garrido 2009a, b) lead to nearly identical predictions. The EIP model is also based on the assumption of a deformation-dependent tube diameter. However, the EIP model assumes that chain stretch is limited by increasing interchain tube pressure caused by thermal fluctuations of the test chain.

From Eq. (15) follows at high Weissenberg numbers $Wi = \dot{\varepsilon}\tau_R$ (with elongational strain rate $\dot{\varepsilon}$) and large deformations, when the equilibrium stretch is reached and $\partial\lambda/\partial t = 0$ that the square of molecular stress f is proportional to the square root of Wi and inverse proportional to the square of the polymer fraction,

$$f^2 = \phi^{-2}\sqrt{5Wi} \tag{17}$$

In this asymptotic limit and neglecting the glass transition, the tensile stress is expected to reach a value of,

$$\sigma = 5G_N f^2 = 5G_N\phi^{-2}\sqrt{5Wi} \tag{18}$$

From Eq. (18) and considering that $G_N = G_{Nm}\phi^2$, the universal relation for the high Wi tensile stress of melts and solutions is obtained,

$$\sigma = 5G_{Nm}\sqrt{5Wi} \tag{19}$$

with G_{Nm} being the plateau modulus of the melt. Eq. (19) is similar to the universal relation of Narimissa et al. (2020) as derived for the EIP model.

Comparison of experimental data and model predictions

In the following, we compare predictions of ERS model, Eqs. (10) and (15), with experimental evidence. We recall that the model is based exclusively on the linear-viscoelastic characterization of the polymer systems and the stretch relaxation time τ_R.

Elongational stress growth coefficient

Figure 3 presents the elongational stress growth coefficient $\eta_E^+(t)$ as a function of time t for Lin180, Star20, and Star90 together with predictions of the ERS model and the Doi–Edwards IA model. Good agreement of data and predictions of the ERS model within experimental accuracy is obtained. Minor discrepancies exist at the low strain rate of $\dot{\varepsilon} = 0.003\ \mathrm{s}^{-1}$ between the steady-state viscosity measured and predicted for Lin180 (prediction too low) and Star90

(prediction too high). At the highest strain rate investigated, $\dot{\varepsilon} = 0.2\ \text{s}^{-1}$, the data of Lin180 and Star90 show a maximum. At least for Lin180, this is unexpected and is most likely an experimental artefact.

In Fig. 4a, data and predictions of the elongational stress growth coefficient $\eta_E^+(t)$ for all 3 polymer systems are presented in the same plot. Data and predictions of Lin180, Star20, and Star90 superimpose for $\dot{\varepsilon} \geq 0.01\ \text{s}^{-1}$ when the stretch-related Weissenberg number $Wi_R = \dot{\varepsilon}\tau_R$ reaches values larger than 1. For the lowest strain rate of $\dot{\varepsilon} = 0.0003\ \text{s}^{-1}$, the presence of the branch point restricting reptation in the polymer stars prolongs terminal relaxation and increases the zero-elongation viscosity. The effect is more pronounced for Star90 due to its longer arm than for Star20. The elongational viscosity as a function of the elongation rate $\dot{\varepsilon}$ is shown in Fig 4b and illustrates the convergence of the elongational viscosities of Lin180 and the star polymers at higher strain rates. We note that the dilution effect of the short sidearm of Star20 vanishes at higher elongation rates as predicted by the universal relation (19), i.e., the elongational stress becomes independent of the degree of dilution in the limit of fast deformations. Concerning Star90, we recall that the ratio of τ_d/τ_R is much larger for Star90 than for Lin180 (Table 1), which translates into the orientational Weissenberg number $Wi_d = \dot{\varepsilon}\tau_d$ of Star90 being much larger than the Weissenberg number $Wi_R = \dot{\varepsilon}\tau_R$ relevant for stretch. When Wi_R reaches a value of $Wi_R = 1$ and stretching of the chain begins, the arms of Star90 are already highly oriented and aligned in the flow direction, i.e., Star90 has already the appearance of a quasi-linear entity, with one arm being either in positive or negative stretching direction, while the two other arms are oriented parallel in the direction opposite to the first arm. This orientational effect is seen in the elongational viscosities already at $\dot{\varepsilon} = 0.003\ \text{s}^{-1}$ (Fig. 4b): With $Wi_R < 1$ for Lin180 and Star20, and $Wi_R \approx 1$ for Star90, there is no significant chain stretch at this elongation rate, while due to orientation, the elongational viscosity of Star20 ($Wi_d = 5$) and of Star90 ($Wi_d = 11$) measured is below the viscosity of Lin180 ($Wi_d = 2$).

Relaxation after steady elongational flow

Huang et al. (2016) investigated stress relaxation when after start-up flow with $\dot{\varepsilon}_0 = 0.03\ \text{s}^{-1}$ the elongation was stopped

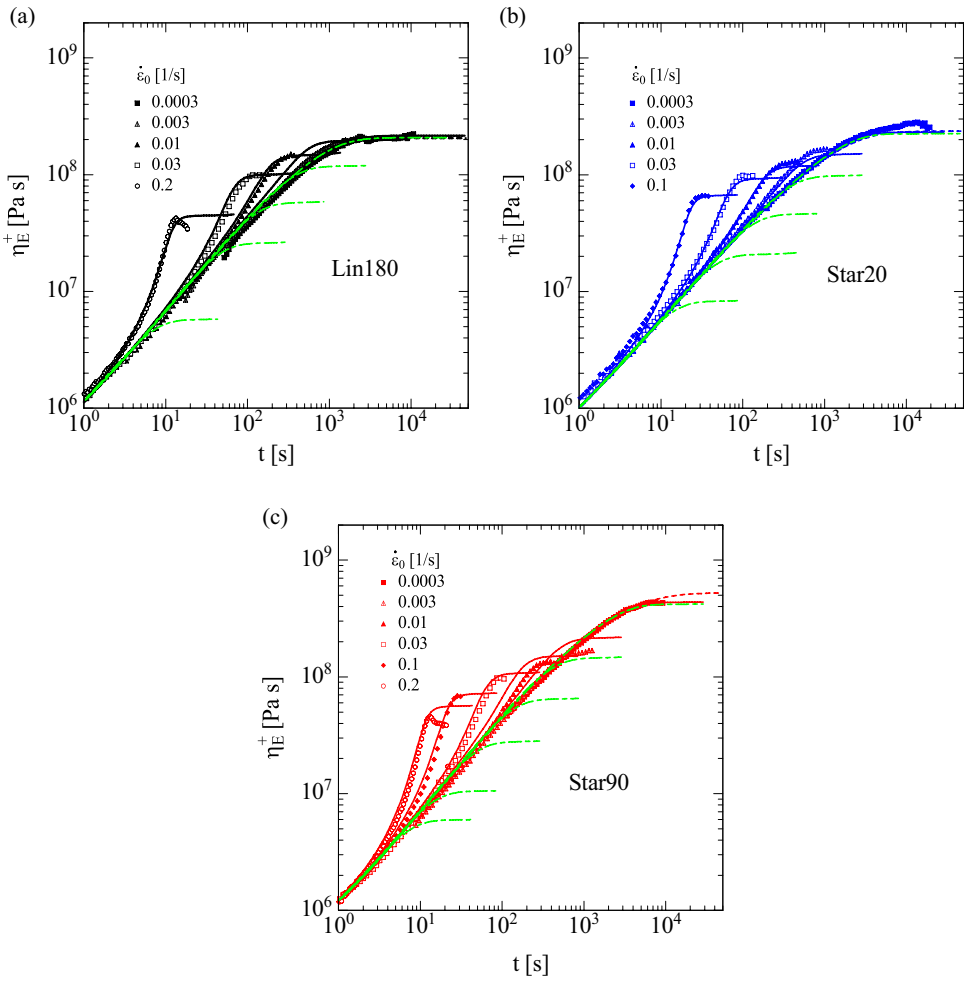

Fig. 3 Data (symbols) and predictions of ERS model (lines) of elongational stress growth coefficient $\eta_E^+(t)$ for **a** Lin180, **b** Star20, and **c** Star90. Short-dashed lines indicate the linear-viscoelastic elongational stress growth coefficient. Long-short dashed lines are predictions of the DE IA model

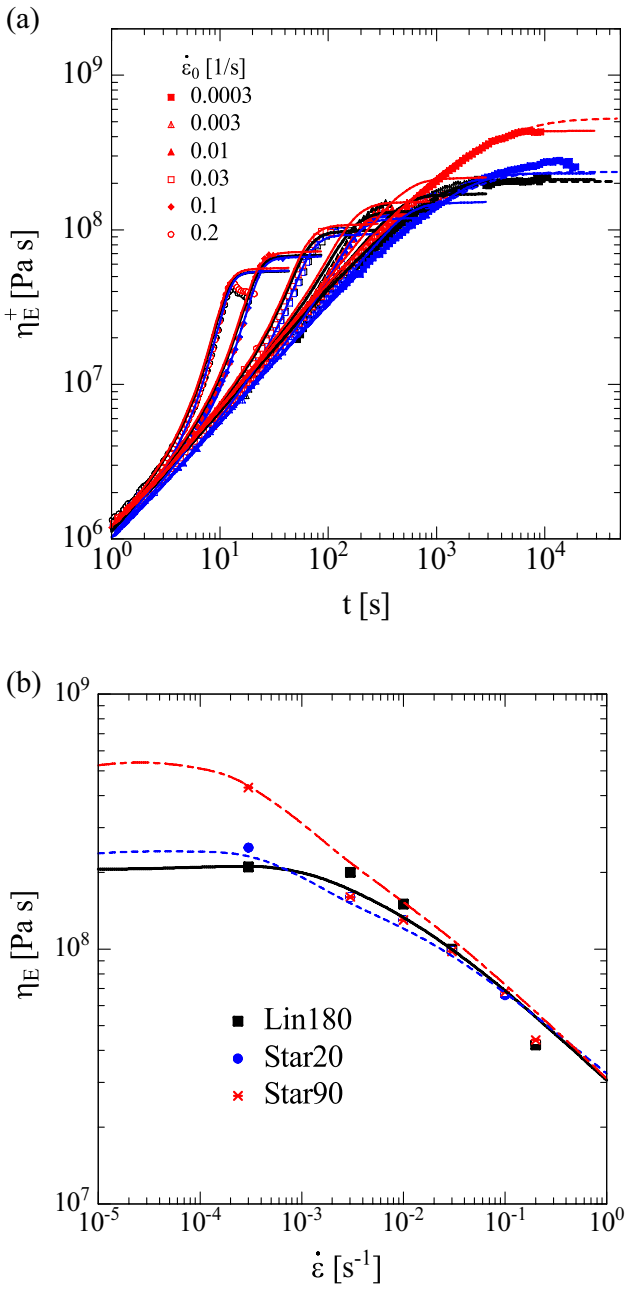

Fig. 4 **a** Data (symbols) and predictions of ERS model (lines) of elongational stress growth coefficient $\eta_E^+(t)$ for Lin180, Star20, and Star90. Short-dashed lines indicate the linear-viscoelastic elongational stress growth coefficients. **b** Data (symbols) and predictions of ERS model (lines) of elongational viscosity $\eta_E(\dot{\epsilon})$ for Lin180 (full line), Star20 (dashed line), and Star90 (long-short dashed line)

at Hencky strain of $\varepsilon = 3.2$. Stress relaxation is reported as $\eta_E^-(t)$, i.e., the stress measured is divided by the elongation rate $\dot{\epsilon}_0 = 0.03s^{-1}$ applied before the flow was stopped. Figure 5a shows the extensional stress growth/decay coefficient as a function of time together with predictions of the ERS model for Lin180. In Fig. 5b, only the decay part is presented by setting the time when relaxation starts as $t = 0$. Excellent agreement between data and model is found. The prediction of the DE IA model is also shown in Fig. 5, which allows separating fast stretch relaxation governed by the Rouse stretch relaxation time τ_R from the long-time relaxation of orientation according to the disengagement time τ_d. This is demonstrated in Fig. 5b by the difference between prediction of the ERS model, $\eta_{ERS}^-(t)$, and the DE IA model, $\eta_{DEIA}^-(t)$, i.e., $\eta_{ERS}^-(t) - \eta_{DEIA}^-(t)$: the effect of chain stretch has totally vanished after a relaxation time of about $3\tau_R$.

Stress relaxation for Star20 and Star90 are presented in Figs. 6 and 7 in comparison to the relaxation of Lin180. As already discussed by Huang et al. (2016), relaxation of Star20 follows the relaxation of Lin180 only for about 15 s after cessation of elongation (Fig. 6). At longer relaxation times, $\eta_E^-(t)$ of Star20 drops off faster than $\eta_E^-(t)$ of Lin180 until the slower terminal relaxation of Star20 sets in. On the other hand, the relaxation curves of Lin180 and Star90 superimpose up to a relaxation time of about 500 s, and then the longer terminal relaxation of Star90 becomes evident. Also shown in Figs. 6 and 7 are predictions of the ERS model. While predictions agree with the initial relaxation of Star20 and Star90, they fail at longer relaxation times. Considering the excellent agreement of experimental data and predictions for the stars in the start-up of elongational flow (Fig. 4) as well as the excellent agreement of data and model predictions for Lin180 in both start-up flow and relaxation (Fig. 5), this is quite surprising. The origin of this disagreement is found in the relaxation of orientation according to the DE IA model, also shown in Figs. 6 and 7: as clearly seen in Figs. 6b and 7b, orientational relaxation observed experimentally is faster than predicted by the DE IA model. This conclusion is substantiated by considering the difference between the prediction of the ERS model and the DE IA model, $\eta_{ERS}^-(t) - \eta_{DEIA}^-(t)$, which is also shown in Figs. 6b and 7b. For both Star20 (Fig. 6b) and Star90 (Fig. 7b), $\eta_{ERS}^-(t) - \eta_{DEIA}^-(t)$ is nearly identical to $\eta_{ERS}^-(t) - \eta_{DEIA}^-(t)$ of Lin180, which means that the effect of chain stretch vanishes for the stars and the linear melt in the same way, in line with the same stretch relaxation time of the three polymer systems. SANS data of relaxation of a stretched symmetric three-arm star melt as reported by Mortensen et al. (2021) show also that initially stretch relaxation occurs as in a linear chain, followed by orientational rearrangement of the two arms, which are oriented parallel to each other in the flow direction and in the opposite direction to the third arm. Therefore, it is likely that stars feature an additional relaxation effect, which is not present in linear polymers and which speeds up the orientational relaxation relative to the expectations of the ERS model. We note that this is a nonlinear-viscoelastic relaxation effect, which should not be confounded with the linear-viscoelastic stress relaxation of stars being slowed down by arm retraction relative to

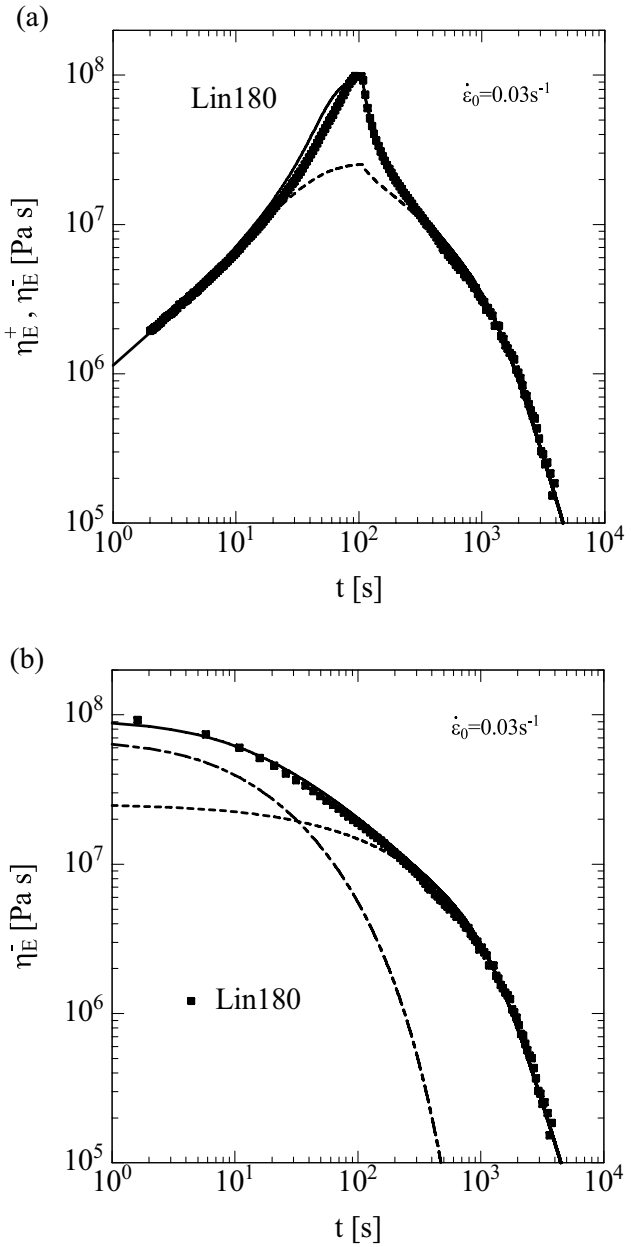

Fig. 5 Comparison of data (symbols) and predictions of ERS model (full lines) of elongational stress growth/decay coefficients $\eta_E^+(t)$ and $\eta_E^-(t)$ for Lin180. The start-up flow with constant strain rate $\dot{\varepsilon} = 0.03s^{-1}$ is stopped at Hencky strain $\varepsilon = 3.2$, followed by stress relaxation. Short-dashed lines are predictions of the DE IA model. In **b** time $t = 0$ is defined as the time when relaxation starts. The difference between predictions of the ERS and the DE IA model, $\eta_{\mathrm{ERS}}^-(t) - \eta_{\mathrm{DEIA}}^-(t)$, is indicated in **b** by the long-short dashed line

the relaxation of linear melts with the same span molecular weight (Frischknecht et al. 2002). Indeed, the terminal stress relaxation of Star 20 and Star90 is slower than of Lin180, as seen in Figs. 6 and 7.

In order to account for the faster orientational relaxation of the stars, we assume that a fraction α of the stress decay coefficient relaxes faster than expected by the ERS model, while a fraction $1-\alpha$ of the orientation relaxes as predicted by the ERS model. The experimentally observed elongational stress decay coefficient $\eta_E^-(t)$ can be described quantitatively by the empirical relation

$$\eta_E^-(t) = \alpha \ \ \exp\left[-\left(t-t_0\right)/\tau_{\mathrm{or}}\right] \ \ \eta_{\mathrm{ERS}}^-(t) + (1-\alpha)\eta_{\mathrm{ERS}}^-(t) \tag{20}$$

$\eta_{\mathrm{ERS}}^-(t)$ is the elongational stress decay coefficient of the ERS model according to the stress Eq. (10), t_0 the time when relaxation starts at $\varepsilon = 3.2$, and τ_{or} is the relaxation time of the additional relaxation process. For Star20, excellent fit of the relaxation data is obtained for values of $\alpha = 0.30$ and $\tau_{\mathrm{or}} = 30$ s (Fig. 6c and d), while for Star90 the corresponding parameters are $\alpha = 0.45$ and $\tau_{\mathrm{or}} = 300$ s (Fig. 7c and d). Equation (20) is obtained by replacing the DE IA tensor $\mathbf{S}_{\mathrm{DE}}^{\mathrm{IA}}(t,t')$ in the stress Eq. (10) for times $t \geq t_0$ by

$$\mathbf{S}_{\mathrm{DE}}^{\mathrm{IA}}(t,t') = \mathbf{S}_{\mathrm{DE}}^{\mathrm{IA}}\left(t_0,t'\right)\left[\alpha \exp\left(-\left(t-t_0\right)/\tau_{\mathrm{or}}\right) + (1-\alpha)\right] \tag{21}$$

resulting in a stress equation for $\sigma(t \geq t_0)$ of the form

$$\begin{aligned}&\sigma(t \geq t_0) = \\ &\alpha \exp\left(-\left(t-t_0\right)/\tau_{\mathrm{or}}\right) \int_{-\infty}^{t_0} \frac{\partial G\left(t-t'\right)}{\partial t'} f^2(t,t') \ \ \mathbf{S}_{\mathrm{DE}}^{\mathrm{IA}}\left(t_0,t'\right)dt' \\ &+ (1-\alpha) \int_{-\infty}^{t_0} \frac{\partial G\left(t-t'\right)}{\partial t'} f^2(t,t') \ \ \mathbf{S}_{\mathrm{DE}}^{\mathrm{IA}}\left(t_0,t'\right)dt'\end{aligned} \tag{22}$$

The additional orientational relaxation process of the DE IA tensor $\mathbf{S}_{\mathrm{DE}}^{\mathrm{IA}}(t,t')$ is only active during relaxation. It is suppressed during start-up of flow, possibly due to tension in the chain. It becomes active as soon as stretch is reduced by relaxation.

Conclusions

Star polymers with three arms are the simplest example of branched polymers. As shown by Huang et al. (2016), a symmetric star (Star90), an asymmetric star (Star20), and a linear polystyrene melt (Lin180) with the same molecular weight of the backbone show the same elongational stress growth coefficient and reach the same elongational steady-state viscosity in fast flows, i.e., at Weissenberg numbers $Wi_R = \dot{\varepsilon}\tau_R > 1$. According to our analysis, in the start-up of the elongational flow of stars, the effects from the arm and the branch point are shielded: for Star20 with an arm length of about one entanglement, the arm acts as a diluent on the time scale of the backbone, and Star20 behaves like a linear polymer diluted to a volume fraction of $\phi = 0.89$. For Star90, the ratio of disengagement time to stretch relaxation time is $\tau_d/\tau_R = 27$ compared to $\tau_d/\tau_R = 6$ for Lin180 with the same span molecular weight. Therefore, when Wi_R reaches a

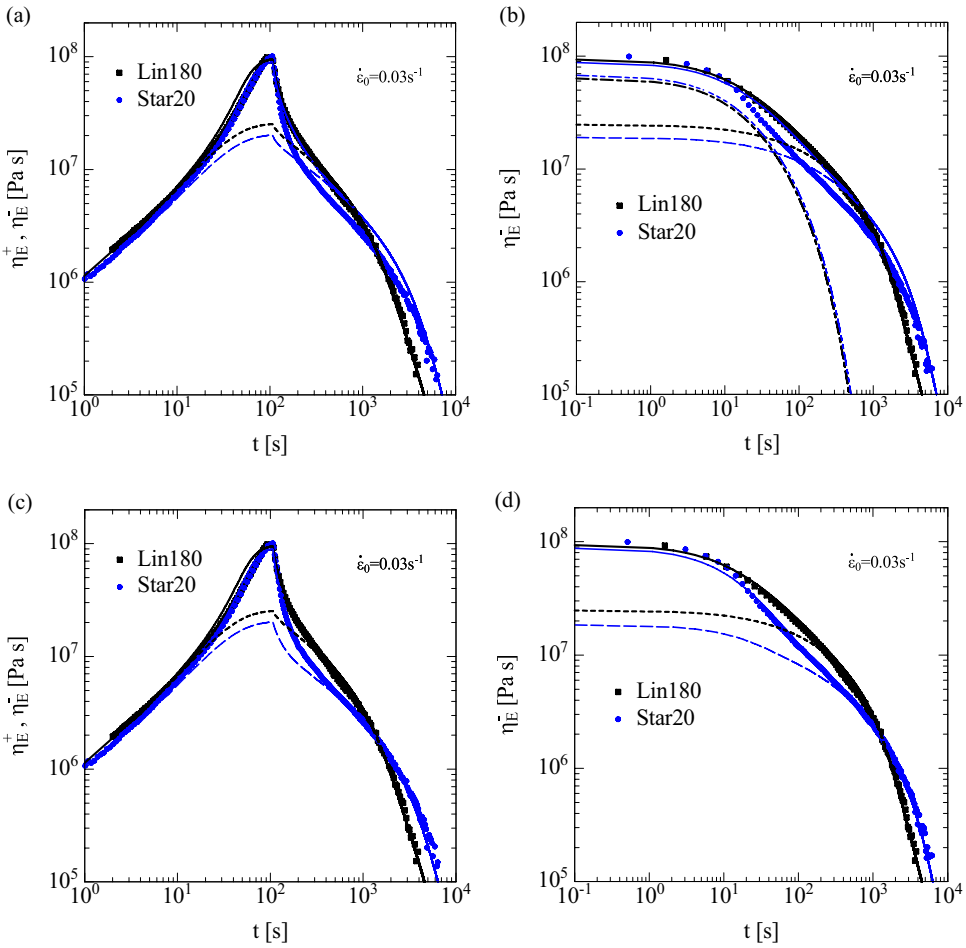

Fig. 6 Comparison of data (symbols) and predictions (full lines) of elongational stress growth/decay coefficients $\eta_E^+(t)$ and $\eta_E^-(t)$ for Lin 180 and Star20. The start-up flow with constant strain rate $\dot{\varepsilon} = 0.03\ \ s^{-1}$ is stopped at Hencky strain $\varepsilon = 3.2$, followed by stress relaxation. In (b) and (d) time $t = 0$ is defined as the time when relaxation starts. Dashed lines are predictions of the DE IA model. **a** and **b** Predictions of ESR model, Eq. (10). In (b), also the differences between prediction of the ERS model and the DE IA model, $\eta_{ERS}^-(t) - \eta_{DEIA}^-(t)$, for Lin180 and Star20 (long-short dashed lines) are shown. **c** and **d** Predictions of ESR model, Eq. (10), plus additional relaxation process according to Eq. (20) with $\alpha = 0.30$ and $\tau_{or} = 30\ \ s$

value of $Wi_R = 1$ and stretching of the chain begins, the arms of Star90 are already highly oriented and aligned in the flow direction, i.e., Star90 has already the appearance of a linear entity, with one arm being either in positive or negative stretching direction, while the two other arms are oriented parallel in the direction opposite to the first arm. For all three polymer systems, excellent agreement between experimental data of the elongational stress growth coefficient and predictions of the ERS model (Wagner and Narimissa 2021) is obtained, based exclusively on the linear-viscoelastic characterization and the Rouse stretch relaxation time of Lin180.

However, stress relaxation following the steady elongational flow of the stars depends on the presence of the branch point and the length of the arm and is different from stress relaxation of Lin180. Our analysis shows that this discrepancy is related to the relaxation of the orientation of the stars, and not to the relaxation of stretch. A new process regarding orientational relaxation of the stars is identified: while a fraction $1-\alpha$ of the orientation of the stars relaxes as expected for a linear chain, a fraction α relaxes much faster. The additional orientational relaxation can be quantified by an orientational relaxation time τ_{or}. For Star20, the parameters of the additional relaxation process are $\alpha = 0.30$ and $\tau_{or} = 30\ \ s$, while for Star90 the corresponding parameters are $\alpha = 0.45$ and $\tau_{or} = 300\ \ s$. The additional process of orientation relaxation is only active during relaxation. It is suppressed during the start-up of flow, possibly due to tension in the chain, and it becomes active as soon as the stretch is reduced by relaxation. Our analysis is in agreement with the SANS data of relaxation of a stretched symmetric three-arm star melt as reported by Mortensen et al. (2021), showing that initially stretch relaxation occurs as for linear chains, followed by orientational rearrangement of arms "1" and "2," which are oriented parallel to each other in the flow direction and in the opposite direction to arm "3." This reorientational process of star relaxation is not present in linear polymers and speeds up orientational relaxation. While it is plausible that the parameters α and τ_{or} of the additional orientational relaxation process are larger for the symmetric Star90 than the asymmetric Star20, we are not yet in a position to relate these parameters quantitatively to the molecular characteristics of the stars. However, we note that the parameter α of Star90 is roughly $\alpha \cong 0.5$. From Eq. (20) and for relaxation times $t - t_0 >> \tau_{or}$, the stress decay coefficient $\eta_E^-(t)$ is approximately $\eta_E^-(t) \cong \eta_{DEIA}^-(t)/2 = \frac{1}{[1/\eta_{DEIA}^-(t) + 1/\eta_{DEIA}^-(t)]}$, i.e. orientational

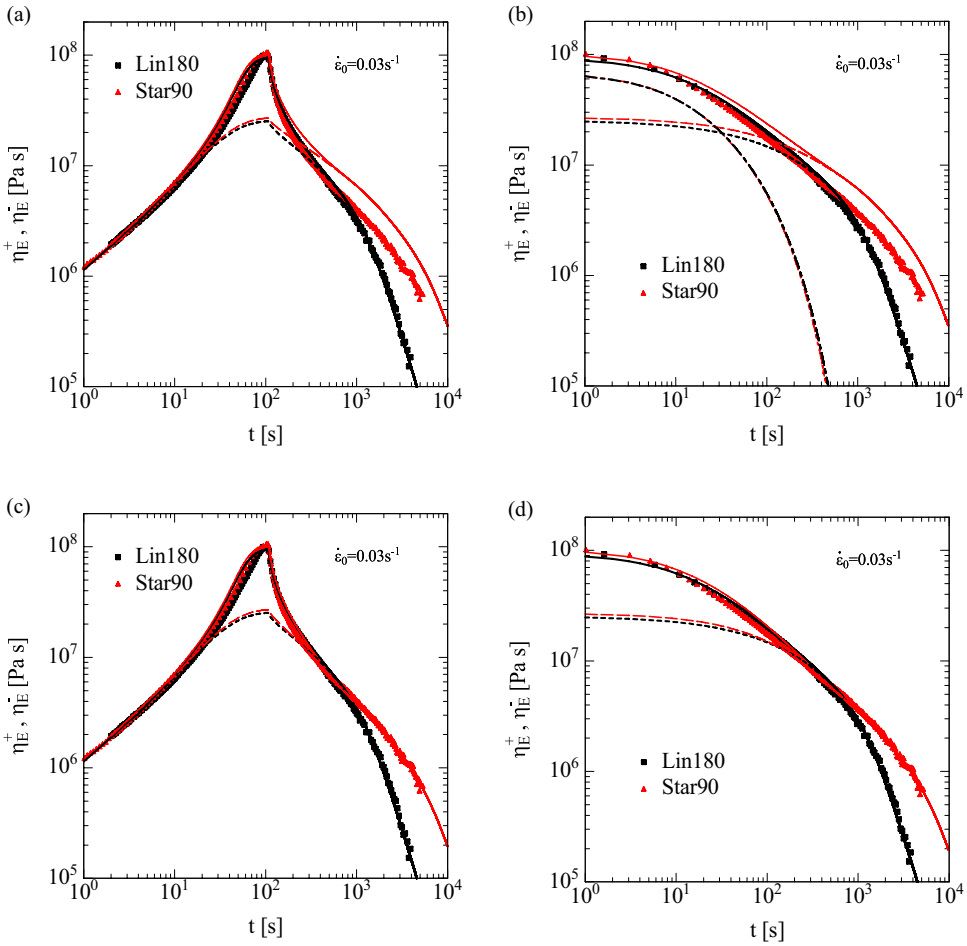

Fig. 7 Comparison of data (symbols) and predictions (full lines) of elongational stress growth/decay coefficients $\eta_E^+(t)$ and $\eta_E^-(t)$ for Lin 180 and Star90. The start-up flow with constant strain rate $\dot{\varepsilon} = 0.03\ \text{s}^{-1}$ is stopped at Hencky strain $\varepsilon = 3.2$, followed by stress relaxation. In (b) and (d) time $t = 0$ is defined as the time when relaxation starts. Dashed lines are predictions of the DE IA model. **a** and **b** Predictions of ESR model, Eq. (10). In (b), also the differences between prediction of the ERS model and the DE IA model, $\eta_{\text{ERS}}^-(t) - \eta_{\text{DEIA}}^-(t)$, for Lin180 and Star90 (long-short dashed lines) are shown. **c** and **d** Predictions of ESR model Eq. (10), plus additional relaxation process according to Eq. (20) with $\alpha = 0.45$ and $\tau_{or} = 300$ s.

relaxation of Star90 can be considered resulting from the addition of the simultaneous relaxation rates of two linear backbones, one made up of arms "1" and "3," the other of arms "2" and "3." Further relaxation experiments on branched polymers with well-defined topology will be needed to characterize this new orientational relaxation process in more detail and to relate it quantitatively to the molecular structure. Also, the implications on the orientational relaxation of more complicated branched structures (comb polymers and randomly branched topologies) need to be investigated.

Acknowledgements The authors acknowledge the financial support from the Ministry of Science and Technology of China (MOST, Grant no.: QN2021030003L).

Funding Open Access funding enabled and organized by Projekt DEAL.

References

Bach A, Rasmussen HK, Hassager O (2003) Extensional viscosity for polymer melts measured in the filament stretching rheometer. J Rheol 47:429–441

Dealy JM, Read DJ, Larson RG (2018) Structure and rheology of molten polymers: from structure to flow behavior and back again. Carl Hanser Verlag GmbH Co KG, München

Doi M, Edwards SF (1978) Dynamics of concentrated polymer systems. Part 3.- The Constitutive Equation. J Chem Soc Faraday Trans 74:1818-1832

Doi M, Edwards SF (1979) Dynamics of concentrated polymer systems. Part 4.- Rheological Properties. J Chem Soc Faraday Trans 75:38-54

Frischknecht AF, Milner ST, Pryke A, Young RN, Hawkins R, McLeish TCB (2002) Rheology of three-arm asymmetric star polymer melts. Macromolecules 35:4801–4820

Huang Q, Agostini S, Hengeller L, Shivokhin M, Alvarez NJ, Hutchings LR, Hassager O (2016) Dynamics of star polymers in fast extensional flow and stress relaxation. Macromolecules 49:6694–6699

Huang Q, Alvarez NJ, Matsumiya Y, Rasmussen HK, Watanabe H, Hassager O (2013) Extensional rheology of entangled polystyrene solutions suggests importance of nematic interactions. ACS Macro Lett 2:741–744

Huang Q, Mednova O, Rasmussen HK, Alvarez NJ, Skov AL, Almdal K, Hassager O (2013) Concentrated polymer solutions are different from melts: role of entanglement molecular weight. Macromolecules 46:5026–5035

Ianniruberto G, Marrucci G (2013) Entangled melts of branched PS behave like linear PS in the steady state of fast elongational flows. Macromolecules 46:267–275

Ianniruberto G, Marrucci G, Masubuchi Y (2020) Melts of linear polymers in fast flows. Macromolecules 53:5023–5033

Isaki T, Takahashi M, Urakawa O (2003) Biaxial damping function of entangled monodisperse polystyrene melts: comparison with the Mead-Larson-Doi model. J Rheology 47:1201–1210

Marrucci G, de Cindio B (1980) The stress relaxation of molten PMMA at large deformations and its theoretical interpretation. Rheol Acta 19:68–75

Menezes E, Graessley W (1982) Nonlinear rheological behavior of polymer systems for several shear-flow histories. J Poly Sci Part B: Poly Phys 20:1817–1833

Milner ST, McLeish TCB (1997) Parameter-free theory for stress relaxation in star polymer melts. Macromolecules 30:2159–2166

Mortensen K, Borger AL, Kirkensgaard JJK, Garvey CJ, Almdal K, Dorokhin A, Huang Q, Hassager O (2018) Structural studies of three-arm star block copolymers exposed to extreme stretch suggests persistent polymer tube. Phys Rev Lett 120:[207801]. https://doi.org/10.1103/PhysRevLett.120.207801

Mortensen K, Borger AL, Kirkensgaard JJK, Huang Q, Hassager O, Almdal K (2021) Small-angle neutron scattering study of the structural relaxation of elongationally oriented, moderately stretched three-arm star polymers. Phys Rev Lett 127(17):[177801]. https://doi.org/10.1103/PhysRevLett.127.177801

Narimissa E, Huang Q, Wagner MH (2020a) Elongational rheology of polystyrene melts and solutions: concentration dependence of the interchain tube pressure effect. J Rheol 64:95–110

Narimissa E, Poh L, Wagner MH (2021) Elongational viscosity scaling of polymer melts with different chemical constituents. Rheol Acta 60:163–174

Narimissa E, Schweizer T, Wagner MH (2020b) A constitutive analysis of nonlinear shear flow. Rheol Acta 59:487–506

Narimissa E, Wagner MH (2019) Review on tube model based constitutive equations for polydisperse linear and long-chain branched polymer melts. J Rheol 63:361–375

Nielsen JK, Rasmussen HK, Denberg M, Almdal K, Hassager O (2006) Nonlinear branch-point dynamics of multiarm polystyrene. Macromolecules 39:8844–8853

Osaki K, Nishizawa K, Kurata M (1982) Material time constant characterizing the nonlinear viscoelasticity of entangled polymeric systems. Macromolecules 15:1068–1071

Takahashi M, Isaki T, Takigawa T, Masuda T (1993) Measurement of biaxial and uniaxial extensional flow behavior of polymer melts at constant strain rates. J Rheol 37:827–846

Wagner MH (1990) The nonlinear strain measure of polyisobutylene melt in general biaxial flow and its comparison to the Doi-Edwards model. Rheol Acta 29:594–603

Wagner MH (2014) Scaling relations for elongational flow of polystyrene melts and concentrated solutions of polystyrene in oligomeric styrene. Rheol Acta 53:765–777

Wagner MH, Kheirandish S, Hassager O (2005) Quantitative prediction of transient and steady-state elongational viscosity of nearly monodisperse polystyrene melts. J Rheol 49:1317–1327

Wagner MH, Narimissa E (2021) A new perspective on monomeric friction reduction in fast elongational flows of polystyrene melts and solutions. J Rheol 65:1413–1421

Wagner MH, Narimissa E, Poh L, Shahid T (2021a) Modelling elongational viscosity and brittle fracture of polystyrene solutions. Rheol Acta 60:385–396

Wagner MH, Narimissa E, Shahid T (2021b) Elongational viscosity and brittle fracture of bidisperse blends of a high and several low molar mass polystyrenes. Rheol Acta 60:803–817

Wagner MH, Rolón-Garrído VH (2008) Verification of branch point withdrawal in elongational flow of pom-pom polystyrene melt. J Rheol 52:1049–1068

Wagner MH, Rolon-Garrido VH (2009a) Nonlinear rheology of linear polymer melts: modeling chain stretch by interchain tube pressure and Rouse time. Korea-Aust Rheolol J 21:203–211

Wagner MH, Rolon-Garrido VH (2009b) Recent advances in constitutive modeling of polymer melts. Novel Trends of Rheology III. AIP Conf Proc 1152:16–31. https://doi.org/10.1063/1.3203266

Wagner MH, Rubio P, Bastian H (2001) The molecular stress function model for polydisperse polymer melts with dissipative convective constraint release. J Rheol 45:1387–1412

Wagner MH, Schaeffer J (1992) Nonlinear measures for general biaxial extension of polymer melts. J Rheol 36:1–26

Wagner MH, Yamaguchi M, Takahashi M (2003) Quantitative assessment of strain hardening of low-density polyethylene melts by the molecular stress function model. J Rheol 47:779–793

Winter HH, Mours M (2006) The cyber infrastructure initiative for rheology. Rheol Acta 45:331–338